Rolling Contact Between Rigid Cylinder and Semi-Infinite Elastic Body With Sliding and Adhesion

S. Hao
ASME Member
e-mail: suhao@northwestern.edu

L. M. Keer
ASME Fellow
e-mail: l-keer@northwestern.edu

Department of Mechanical Engineering,
Northwestern University,
Evanston, IL 60208

Based on a hybrid superposition of an indentation contact and a rolling contact an analytical procedure is developed to evaluate the effects of surface adhesion during steady-state rolling contact, whereby two analytic solutions have been obtained. The first solution is a Hertz-type rolling contact between a rigid cylinder and a plane strain semi-infinite elastic substrate with finite adhesion, which is a JKR-type rolling contact but without singular adhesive traction at the edges of the contact zone. The second solution is of a rolling contact with JKR singular adhesive traction. The theoretical solution indicates that, when surface adhesion exists, the friction resistance can be significant provided the external normal force is small. In addition to the conventional friction coefficient, the ratio between friction resistance force and normal force, this paper suggests an "adhesion friction coefficient" which is defined as the ratio between friction resistance force and the sum of the normal force and a function of maximum adhesive traction per unit area, elastic constant of the substrate, and contact area that is characterized by the curvature of the roller surface. [DOI: 10.1115/1.2736431]

Keywords: rolling-contact, friction coefficient, adhesion, contact mechanics

1 Introduction

Contact friction is an issue in almost all fields in engineering science (see, e.g. [1–4]). The problems of rolling-contact with adhesion at small scales recently became a subject with increasing interest in the research and application of micronanotribology [5–9]. A remaining challenge among others is to obtain predictive theoretical solutions for quantitatively specifying the effects of adhesion during rolling contact. Most existing analyses, e.g. [10,11], emphasize sliding and tangential friction while expression of the normal stress from the static problem is borrowed to obtain semianalytical solutions. The deviation from the exact solution is not easy to identify, especially with adhesion present.

Based on the analytical methodologies of Muskhelishvili [12] and Johnson [3], in conjunction with the solution strategies of Achenbach et al. [13] for the shear Dugdule crack [14] and Maugis [4] for indent contact with adhesion, this paper introduces a procedure to obtain an exact solution of the steady-state rolling contact with adhesion and/or sliding, using a hybrid superposition.

The history of contact mechanics and its state-of-the-art have been carefully reviewed, e.g., in [3,4]. Hertz [1] first derived the relationships among normal pressure, contact area, and contact-induced penetration depth for frictionless contact between two elastic ellipsoids, omitting the effects of adhesion. The Johnson-Kendall-Roberts (JKR) theory [15] first reveals the effect of adhesion analytically for Hertz contact. For hard materials, the Derjaguin-Muller-Toporov (DMT) model [16] incorporates adhesion force as a function of the separation between contact surfaces. However, in this theory the additional deformation caused by the noncontact adhesion is ignored; instead, the deformation field from the Hertz solution is adapted. Hughes and White [17] generalized the framework to describe separation-dependent adhesion between elastic bodies, which includes both "soft contact model" (JKR theory) and "hard contact" (DMT theory). Using the Muskhelishvili-Dugdale model [12,14] of fracture mechanics, Maugis [4] found a closed form solution of the static contact between a semi-infinite plane and a punch with elliptic profile associated with adhesion. The Maugis model has been extended to the cases of cylinder/cylinder and cylinder/plate contact by Barquins [18] and Baney et al. [19], respectively. Sari and co-authors [8] have studied various cases of rolling contact with adhesion by superposition of fracture mechanics solutions and contact solution, neglecting the effects of coupling between normal/shear stress and tangential/normal dislplacement. On other hand, the analytical solution of static contact with adhesion [20] indicates that the effects of normal loading-induced substrate stretch can be significant. For rough, frictional contact, Spence [21] introduced the concept of self-similar contact (SSC), extending the Hertz problem. The two-dimensional frictional punch on a semi-infinite elastic plane with shallow crack has been studied by Hasebe [22,23]. A self-similar frictional contact solution for a nano-indentation has been obtained recently [24,25] based on the methodology of Mossakovskii [26] and others. Further discussions about adhesion-contact and its application can be found, e.g., in [10,20,27–30].

For engineering application, an issue in contact problems with adhesion can concern the definition of resistance to motion. Conventionally the friction coefficient μ is defined as the ratio of the friction resistance force parallel to the rolling or sliding direction and the external normal force. When adhesion is present, the resistance to motion can be significant even without externally imposed pressure [4,27]. An effort is made to clarify this issue based on the obtained solution.

2 Models and Governing Equations

2.1 About Rolling Contact. A rolling contact is somewhat more complicated than static or quasistatic contact. Consider a roller rolling on a surface Ω with an angular velocity ω while a force P normal to Ω, a force Q tangential to Ω, and a moment M^{appl}, *are applied* on the central axial line of the roller, see Fig. 1; also an additional moment M^P is applied on the central axis, which is the toque induced by normal load P, since the system is not symmetric (Fig. 1). By varying the magnitudes and directions

Contributed by the Tribology Division of ASME for publication in the JOURNAL OF TRIBOLOGY. Manuscript received April 2, 2006; final manuscript received January 22, 2007. Review conducted by Andreas A. Polycarpou. Paper presented at the STLE/ASME 2006 International Joint Tribology Conference (TRIB2006), October 22–25, 2006, San Antonio, TX.

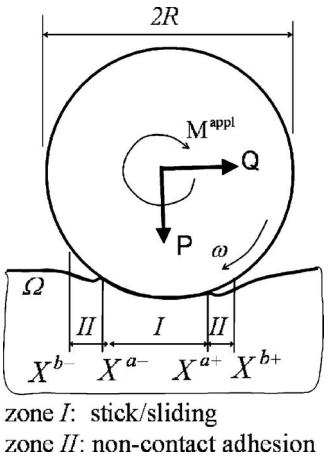

Fig. 1 A rolling contact system with a normal force *P*, a tangential force *Q*, and a moment M^{appl} applied on the central axial line of the roller, where *P* induces additional moment M^P since the system is not symmetric. By varying the magnitudes and directions of *P*, *Q*, and M^{appl}, one obtains different cases of rolling contacts that can be classified into three categories: (1) free rolling: $M^{appl}=0, Q=0$; (2) scratching: $M^{appl}+M^P+RQ=0$ and $\omega=0$; (3) $\omega\neq 0$ and $0<\{|RQ|+|M^{appl}|\}$, which is termed "constraint rolling" in this paper.

of M^{appl} and Q, one obtains different cases of rolling contact that can be classified into three categories: (1) free rolling: $M^{appl}=0$, $Q=0$; (2) scratching: $M^{appl}+M^P+RQ=0$, and $\omega=0$; (3) $0<|M^{appl}|+|RQ|$ and $\omega\neq 0$, which is termed "constraint rolling" in this paper.

Let $R\omega=V$ for constraint rolling, while the roller, Fig. 1, is an infinitely long cylinder. The problem is then a plane strain contact between a rolling cylinder with radius R and a semi-infinite elastic substrate. Here, the cylinder is under normal pressure P and lateral force Q per unit thickness along the direction perpendicular to the plane. The adhesion is taken to occur both inside of the contact zone (zone I) and outside of the contact zone (zone II).

2.2 About Adhesion During Contact. The physics of "friction" or "contact" always relates to the length scale considered. Figure 2(*a*) illustrates a hierarchical structure of a contact problem; a macroscopic contact between two surfaces is actually the adhesion and friction between asperities on the surfaces at microscales. At the atomic scale, a contact is essentially a discontinuity between two periodic atoms arrays and the contact between two atoms means that λ_N, the normal distance between centers of the atoms, deviates from λ_N^{atom}, an equilibrium distance without interacting force. λ_N^{atom} is usually on the same order as the lattice constant. When $\lambda_N<\lambda_N^{atom}$, the interatomic force is repulsive, otherwise it is attractive. Hence, a tribological "contact" occurs when the normal distance λ_N between two contact surfaces is equal or less than a character distance λ_N^0, where the "surface" is defined as the centers of the atoms that form the surface layer of a solid body and the character distance λ_N^0 can be, e.g., the distance between the surfaces within which an attractive interaction exists, where the definition of λ_N^0 specifies a "contact." When λ_N^0 is, e.g., the atomic equilibrium distance λ_N^{atom}, then in the corresponding "contact zone" there will be only repulsive traction or no traction. Alternatively, when the distance λ_N^0 is defined to be equal to a "cutoff" distance λ_N^{cutoff}, beyond which adhesion may be ignored (see Fig. 2(*b*)), then adhesive traction takes place only within the contact zone, as described by the JKR model [15]. Under this situation, the noncontact adhesion zone II illustrated in Fig. 1 vanishes. Usually λ_N^{cutoff} is of the order of $10^{-1}-10^{1}$ nm.

In general, a surface adhesion can be expressed in the form as

$$T=\begin{cases}\varphi_1(\lambda_N)\leqslant T_0 & 0\leqslant\lambda_N\leqslant\lambda_N^0\\ \varphi_2(\lambda_N) & \lambda_N^0<\lambda_N\leqslant\lambda_N^{cutoff}\\ 0 & \lambda_N>\lambda_N^{cutoff}\end{cases} \tag{1}$$

where $\varphi_1(\lambda_N)$ and $\varphi_2(\lambda_N)$, respectively, are functions of λ_N, the normal distance between the surface pair; λ_N^{cutoff} is a "cutoff" distance, beyond which adhesion becomes ignorable. In (1) the first line defines "contact," which states that within a contact zone ($0\leqslant\lambda_N\leqslant\lambda_N^0$) the traction between two contact surfaces can be either compressive or attractive with the amplitude less than T_0. The combination of $\varphi_1(\lambda_N)$ and $\varphi_2(\lambda_N)$ defines a traction-separation law which is similar to the interfacial cohesive law introduced by Needleman [31], which can be, e.g., a linear relation characterized by the maximum adhesion T_0 and the rate of decay T_1,

$$\varphi(\lambda_N)=T_0-T_1\lambda_N \quad \text{for } 0\leqslant\lambda_N\leqslant\frac{T_0}{T_1} \tag{2}$$

or the derivative of the Lennard-Jones-type potential,

$$\varphi(\lambda_N)=\frac{d\Phi_{LJ}}{d\lambda_N} \text{ and } \Phi_{LJ}=\varepsilon_0\left[\left(\frac{\sigma_0}{\lambda_N}\right)^{n_1}-\left(\frac{\sigma_0}{\lambda_N}\right)^{n_2}\right] \quad \text{for } 0\leqslant\lambda_N\leqslant\infty \tag{3}$$

in (1)–(3) σ_0, ε_0, λ_N^0, λ_N^{cutoff}, T_0, and T_1 are materials constants. For the potential in (3), $\lambda_N^{cutoff}\Rightarrow\infty$ and n_1, n_2 are determined through the Hamaker integral over the interatomic potential [32,4].

In general, the maximum adhesion T_0 can be expressed in the form of $T_0=k\gamma_S/\lambda_N^{atom}$, where λ_N^{atom} is the atomic equilibrium distance and k is a coefficient with values from 4 to 10 (see Sec. 1.2.4 of [4]).

2.3 Self-Similarity [21]. The steady-state rolling contact to be studied is also assumed to possess dual self-similarities. First, when the roller rolls with constant speed, at different time instances the deformation solution fields are identical if these solutions are defined in the coordinate system attached to the roller. Second, at a given time instance, varying normal pressure leads to a series of self-similar solutions, analogous to the solution obtained by Spence [21] for the Hertz contact problem under progressive loading. For that case the self-similarity refers to the dimensionless field solutions of u_i/l and σ_{ij}/G, which are the functions of dimensionless coordinates X_i/l only; here l is the half-length of a contact zone, X_i is the coordinate originated at the bottom of the indent.

2.4 JKR, DMT, and Other Models of Adhesive Contact. The JKR model [15] is the first mathematically complete contact solution with adhesion and is also referred to as a "soft model" of adhesion contact [4,17]. In this case, when deformation caused by a contact is not ignorable either inside or outside of a contact zone, the corresponding contact zone size will be relatively large and the amplitude of λ_N^{cutoff} in (1) will be relatively small since the latter is a material constant. One can assume that $\lambda_N^{cutoff}=\lambda_N^0$ in (1) and the ratio between λ_N^0 and contact zone size is infinitesimal. Under this situation, the adhesion outside the contact zone is also infinitesimal and a high amplitude of adhesion is required to maintain two contact surfaces sticking together near the two ends inside the contact zone. Such a high adhesive traction is described mathematically as an additional singular term to the Hertz solution in [15], which is similar to the stress intensity factor solution for the mode I Griffith crack tip in linear elastic fracture mechanics. On other hand, the DMT model [16] accounts for the adhesion outside of contact zones but adopts Hertz's deformation solution, which implies that the adhesive traction has no effect on the deformation of the contact surface. Thus, this theory is termed "hard model."

The intellectual merit of JKR theory lies in the introduction of

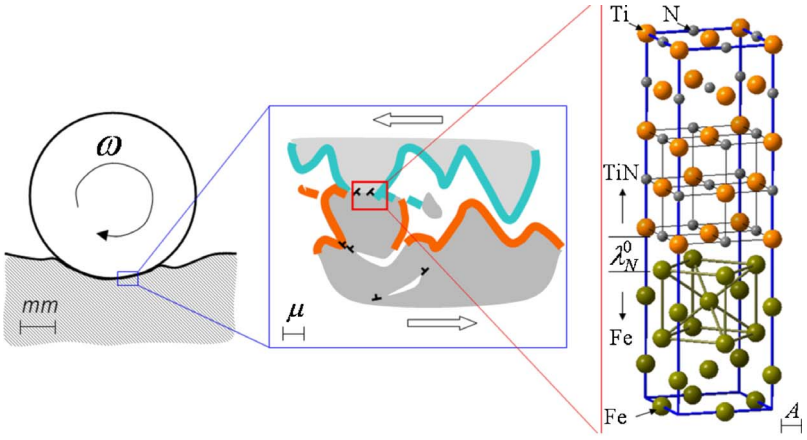

(*a*)

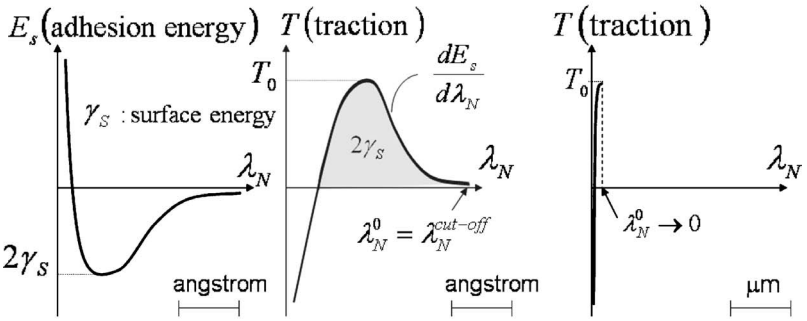

(*b*)

Fig. 2 (*a*) **Hierarchical structure of a tribological process, the right most is the contact/sliding between an iron substrate and a TiN particle at (001) surface, the details of this analysis can be found in the Sec. 4.1 of [32]; (*b*) relationship between adhesion energy, surface energy, and the definition of λ_N^0 for JKR-type adhesion**

adhesion to contact and to reveal the similarity between the adhesive contact solution and crack tip singular solution. According to the solution procedure of a penny-shaped crack with a strip yield zone ahead of the crack tip in the small scale yield fracture mechanics, Maugis obtained the complete analytical solution of the contact between two elastic spheres with an additional noncontact zone enhanced with constant adhesion σ_0 [4], which removes the singular adhesion in JKR theory. When the noncontact adhesion zone becomes infinite and σ_0 vanishes, this solution coincides with Hertz's solution without adhesion. It degenerates to the JKR solution provided the noncontact adhesion zone vanishes. When the deformation field approaches Hertz's solution, it describes the DMT model with constant adhesion σ_0. Hence, Maugis' solution essentially establishes the connections among Hertz's solution, JKR theory, and DMT model for static contact, as illustrated in Fig. 3(*a*).

Although semianalytical solutions of rolling contact, e.g., [10,11], were developed more than a half century ago, it remains a challenge to quantitatively describe the effects of adhesion on rolling/sliding contact accurately. Following the scheme introduced in [4], Baney and Hui [19] obtained a solution of the static contact between cylinders with DMT adhesion. Barquins proposed the procedure using fracture mechanics solutions to study rolling contact with adhesion [18]. This concept has been further developed by Sari and co-workers [8]. In [8] the Carter's rolling/sliding contact problem has been analyzed by the superposition of various crack tip solutions and a contact solution neglecting the coupling between normal/shear stress and tangential/normal displacement. The obtained results agree with static JKR and Maugis' solutions in general. However, as indicated by Sec. 8 of [3], the effect of Possion's ratio is significant for nonadhesion rolling/sliding. Hence, the effect of couplings between normal and transverse field variables can be remarkable for some adhesive rolling contacts, e.g., for the cases at the micron scale as illustrated on the left end of Fig. 2(*a*) or the cases at the nanometer scale where the short-ranged chemical bonding force dominates.

2.5 Proposed Model. In contrast to static problems, in a rolling adhesive contact the system is no longer symmetric; so the corresponding distribution of adhesion and sliding can be quite different from these in static solutions. These distributions, in conjunction with material constants that include the maximum adhesion, Young's modulus, and Poisson's ratio, essentially determine the mesoscopic behaviors of the rolling/sliding contact system.

This paper develops a model to obtain an analytical solution of the steady-state rolling contact; the mathematical singular adhesive tractions at the edges of the contact zone are removed. Instead, the traction-separation law defined by (1) is applied. As illustrated in Fig. 3(*b*), the idea of the proposed solution procedure is inspired by Maugis' static adhesive contact solution and Achenbach et al.'s adhesive shear crack model [13]. The obtained solution degenerates to a rolling contact solution with JKR adhesion when the singular term is taken into account.

In the contact system of Fig. 1, the following approximations are adapted in the analysis of this study:

(a) Rigid cylinder roller, linear elastic substrate;
(b) The roller rotates clockwise with a constant angular velocity ω while the substrate advances horizontally from

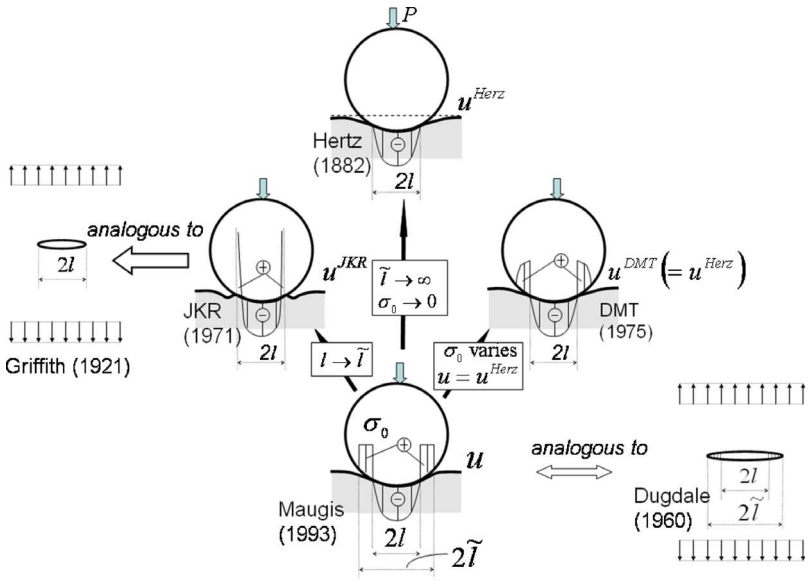

(*a*)

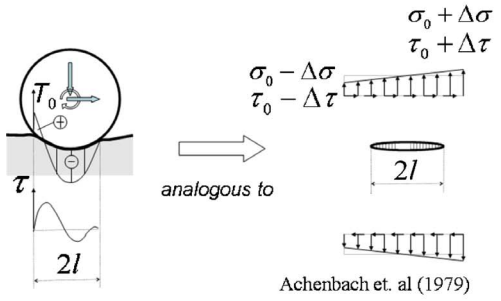

(*b*)

Fig. 3 (*a*) Models of adhesion contact between elastic bodies; (*b*) proposed adhesion contact model for the rolling contact

right to left with a constant speed V; the case of $R\omega = V$ is taken into account first;

(c) Infinitesimal strain;

(d) The effects of inertia and weight are omitted;

(e) The traction-separation relation (1), i.e., $T = T(\lambda_N)$ [17,31], is applied. Furthermore, we first consider the JKR theory without singular adhesion, so

$$\lambda_N^{\text{cutoff}} = \lambda_N^0 \quad \frac{\lambda_N^0}{l} \to 0$$

where l is the half-size of the contact zone; therefore the following simplification is taken:

$$\lambda_N^0 = 0 \tag{4}$$

(f) The effect of adhesion induced bifurcation during progressive load, i.e., the"jumping on" stick discussed in [28], is not taken into account.

(g) Without loss of generality, it is assumed that $M^{\text{appl}} = 0$ in Fig. 1.

According to the approximation (e), the noncontact adhesion zone II in Fig. 1 vanishes, so $X^{b-} = X^{a-}$ and $X^{b+} = X^{a+}$. Under these approximations, the boundary-value problem defined by the contact system in Fig. 1 is solved through the superposition of the displacement-based solutions of two independent boundary-value problems, as illustrated in Fig. 4. The corresponding contact analysis can be divided into the following stages:

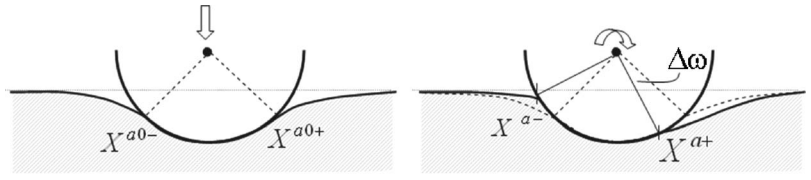

(*a*) (*b*)

Fig. 4 Solution strategy of the rolling-contact with JKR adhesion; superposition of roller indentation (*a*) and adhesion rotation (*b*)

(1) The roller indents the substrate with the depth $\tilde{\Delta}_{\perp}$ at the time instance $\tau=0$, Fig. 4(*a*). Let $2l$ to be the length of the contact zone, i.e., $X^{a0+}-X^{a0-}=2l$, and $\Delta\bar{l}$ is the average elongation of the substrate at the two ends of the indentation-induced contact zone, then the average transverse strain on the contact surface, denoted as ε_{av}, reads

$$\frac{\Delta\bar{l}}{l}=\varepsilon_{\text{av}} \tag{5}$$

(2) The roller rotates clockwise through an angle $\Delta\omega$ while the particles of the substrate surface within $X^{a0-}\leqslant X_1\leqslant X^{a0+}$ adhere to the roller surface until a detachment takes place where the contact zone becomes $X^{a-}\leqslant X_1\leqslant X^{a+}$, illustrated in Fig. 4(*b*). During this rotation, relative sliding between substrate and roller surface is permissible within the contact zone but the substrate material particles at the two ends of the contact zone are presumed to stick to the roller so there is no change in the contact zone size, i.e.,

$$X^{a0+}-X^{a0-}\equiv X^{a+}-X^{a-} \tag{6}$$

which is identical to the approximations (b), i.e., $R\omega=V$ and infinitesimal strain.

(3) When the roller continuously rotates and steadily travels forward, once a detachment occurs at one end of the contact zone, a new attachment is assumed to occur simultaneously at the another end; thus the stick zone size remains constant in the coordinate system $\{X_i\}$ that originated at the intersection of the vertical central line and the bottom of the roller.

(4) During the motion described by (1)–(3), a detachment of the stick-contact is determined by the condition when the maximum normal separation stress in the contact zone is equal to the maximum adhesion T_0 prescribed by (1); this condition can be stated mathematically as follows:

$$\max\{\,\sigma_{22}(X_1)|_{X_2=0};\ X^{a-}\leqslant X_1\leqslant X^{a+}\}=T_0 \tag{7}$$

The mathematical definitions of these two boundary-value problems will be given in the following sections.

2.6 Governing Equations

2.6.1 Galilean Transformation. The contact system of Fig. 1, defined in a two-dimensional spatial Cartesian coordinate system $\{X_1,X_2\}$ where the origin is at the intersection between the vertical central line and the bottom of the roller, can be considered as under a steady-state motion [33] when the approximations (a)–(d) in Sec. 2.5 apply. Let V be the horizontal velocity of the substrate and τ be time, then the Galilean transformation

$$X_1=x_1-V\tau \quad X_2=x_2-R \tag{8a}$$

defines the relation between $\{X_i\}$ and a moving coordinate system $\{x_i\}$ embedded in the substrate. Since the roller is rigid, this contact system forms a boundary value problem in the semi-infinite substrate.

By holding $\{x_1,x_2\}$ fixed, according to (8*a*) $f(\tau,x_i)=f(X_i)$ for an arbitrary function $f(\tau,x_i)$ and applying the chain rule, the time derivative of $f(\tau,x_i)$ yields

$$\frac{\partial f(\tau,x_i)}{\partial\tau}=-V\frac{\partial f(X_i)}{\partial X_1} \tag{8b}$$

Hence, the displacement, velocity, stress, and strain fields defined in the coordinates $\{\tau,x_1,x_2\}$ can be expressed as functions of the coordinates $\{X_1,X_2\}$, which define the "Carter problem" [11] for the rolling contact illustrated in Fig. 1.

2.6.2 Boundary Condition and Equilibrium Solution in Complex Plane. A two-dimensional Cartesian coordinate system $\{X_1,X_2\}$, such as (8*a*), can be represented in the complex plane as by $z=X_1+iX_2$ and $\bar{z}=X_1-iX_2$. In the following analysis, the notations $\text{Re}\{f(z)\}$ and $\text{Im}\{f(z)\}$ denote the real and imaginary parts $f(z)$, respectively, of a complex function; hence, if $f(z)=f_1(z)+if_2(z)$, then $\text{Re}\{f(z)\}=f_1(z)$, $\text{Im}\{f(z)\}=f_2(z)$. Also $\bar{f}(z)=f_1(z)-if_2(z)$.

According to the approximations (a)–(f) in Sec. 2.5, the rolling/sliding contact illustrated in Fig. 1 becomes an elastic equilibrium problem of a semi-infinite plane under given rolling/sliding boundary conditions along the real axis. Let $u_1(t)$ and $u_2(t)$, respectively, be the horizontal and vertical displacements of the real axis embedded in the substrate, where t represents the coordinate along the real axis. Also, let $p(t)$ and $q(t)$, respectively, be the distribution of the normal pressure and shear stress on the real axis, corresponding to the total compression force P and shear force Q, respectively. According to Muskhelishvili (Sec. 113 in [12]), $p(t)$ and $q(t)$ can be calculated by the following relation:

$$p(t)+iq(t)=\frac{\kappa+1}{\kappa}\Phi^{+}(t)+\frac{G(\kappa-1)}{\kappa}\frac{d}{dt}[u_1(t)+iu_2(t)] \tag{9}$$

where G is the shear modulus and κ is the elastic coefficient defined as a function of Poisson's ratio; under plane strain condition it reads $\kappa=3-4v$.

The $\Phi^{+}(t)$ in (9) represents the branch of a stress function $\Phi(z)$ when z approaches the real axis from the upper semi-infinite plane, i.e., $X_2>0$. This stress function is determined by

$$\Phi(z)=\frac{Z(z)}{2\pi i}\int_L\frac{h(t)dt}{Z(t)(t-z)}+Z(z)P_m(z) \tag{10}$$

where $Z(\,)$ and $P_m(\,)$ are functions to be determined, which will be discussed in detail later; the integral of (10) is on the segment L along the entire real axis. When a stress boundary condition is prescribed on L,

$$h(z)=p(z)+iq(z) \tag{11}$$

When a displacement boundary condition is given on L, then

$$h(z)=2G\frac{d}{dz}[u_1(z)+iu_2(z)] \tag{12}$$

For the rolling contact problem in Fig. 1, the displacement boundary condition is given in the contact zone, as illustrated in Fig. 4; the traction free condition is given outside the contact zone so $h(z)$ vanishes. Hence, the integral route L degenerates to the contact zone $X_1^{a-}\leqslant X_1\leqslant X_1^{a+}$ and the stress function is solvable when the displacement $h(z)$ is given.

When $\Phi(z)$ is known, the stress distributions on the entire semi-infinite plane are determined [12]:

$$\sigma_{11}+\sigma_{22}=2[\Phi(z)+\bar{\Phi}(\bar{z})] \tag{13a}$$

$$\sigma_{22}-\sigma_{11}+2i\sigma_{12}=2[(\bar{z}-z)\Phi'(z)-\Phi(z)-\bar{\Phi}(z)] \tag{13b}$$

For the problem of Fig. 1, at infinity $(z\to\infty)$ the following condition should be satisfied:

$$\sigma_{11}=\sigma_{12}=\sigma_{22}=0 \tag{14}$$

Also, the global equilibrium requires that

$$P=\int_L p(t)dt \quad Q=\int_L q(t)dt \tag{15}$$

where L denotes the contact zone. The global moment conservation requires

$$M^{\text{appl}} = \int_L Rq(t)dt + \int_L tp(t)dt \tag{16}$$

The relation (10) and boundary conditions (11), (12), and (14)–(16) are the governing equations to be solved.

3 A Rolling Contact Solution With Adhesion

3.1 Two Boundary Value Problems. The problem addressed in Fig. 1, as discussed in Sec. 2.5, is solved by the superposition of the solutions of the following two boundary-value problems defined in Figs. 4(*a*) and 4(*b*). Using the superscripts I and II to denote the variables associated with the problem I and II, these two boundary-value problem can be stated as below.

Problem I (roller indentation): find $\boldsymbol{u^I}=[u_1^{\text{I}}, u_2^{\text{I}}]$ that satisfies the elastic equilibrium condition and the boundary conditions which specify the motion illustrated in Fig. 4(*a*),

$$u_1^{\text{I}} = \tilde{u}(t) \quad u_2^{\text{I}} = -\delta_\perp + \frac{t^2}{2R} \quad \text{for } X_2 = 0 \ |t| \leqslant l \tag{17}$$

and

$$\sigma_{22}^{\text{I}} = \sigma_{12}^{\text{I}} = 0 \quad \text{for } X_2 = 0 \ |t| > l \tag{18}$$

where $\delta_\perp$ is constant, $\tilde{u}(t)$ is the surface transverse deformation to be determined, t is a coordinate defined as

$$t = X_1 - \bar{l} \quad \bar{l} = \frac{X^{a+} + X^{a-}}{2} \quad l = \frac{X^{a+} - X^{a-}}{2} \tag{19}$$

The coordinate origin ($t=0$) is the geometrically symmetric center of the contact zone size, see Fig. 4(*a*). In (17) and (18) and the analysis hereafter, the superscript I indicates the quantities associated with the problem I and II to the quantities with the problem II to be discussed. In this analysis the quantities with the orders of $o(t^4/R^3)$ are omitted.

Assuming that the surface transverse deformation in (17) can be expressed as a series expansion of a self-similar solution,

$$\tilde{u} = \tilde{u}_{\text{sym}} + \tilde{u}_{\text{skm}} \tag{20}$$

$$\tilde{u}_{\text{sym}} = l\varepsilon_{\text{av}}\left[a_1\left(\frac{t}{l}\right) + a_3\left(\frac{t}{l}\right)^3 + \cdots\right] \tag{21}$$

$$\tilde{u}_{\text{skm}} = \gamma_{\text{sv}}\left[\left(\frac{t}{l}\right)^2 + a_4\left(\frac{t}{l}\right)^4 + \cdots\right] \tag{22}$$

where $\tilde{u}_{\text{sym}}$ is a skew-symmetric function that describes a transverse deformation symmetrical to $t=0$ while $\tilde{u}_{\text{skm}}$ is a symmetric function that characterizes the antisymmetrical part of the transverse displacement $\tilde{u}$; the constants $\varepsilon_{\text{av}}, \gamma_{\text{sv}}, a_1, a_3, a_4, \ldots$ are to be determined. According to (5) and (6) and associated approximations, we know that at $t=\pm l$,

$$\tilde{u}_{\text{sym}} = l\varepsilon_{\text{av}} \ \tilde{u}_{\text{skm}} = 0$$

therefore

$$a_1 = 1 - a_3 \ a_4 = -1 \tag{22a}$$

Problem II (roller stick-rotation): find $\boldsymbol{u^{II}}=[u_1^{\text{II}}, u_2^{\text{II}}]$ that satisfies elastic equilibrium condition and the boundary conditions which specify the motion illustrated in Fig. 4(*b*),

$$u_1^{\text{II}} = \tilde{u}_{\text{skm}} + R\Delta\omega\left[\left(1 - \frac{1}{2}\left(\frac{t}{R}\right)^2 - \frac{\Delta\omega^2}{6}\right) + \frac{t}{R}\frac{\Delta\omega}{2}\right]$$
$$\text{for } X_2 = 0 \ |t| \leqslant l \tag{23}$$

$$u_2^{\text{II}} = R\Delta\omega\left[\frac{\Delta\omega}{2} - \frac{t}{R}\right] \quad \text{for } X_2 = 0 \ |t| \leqslant l \tag{24}$$

where $\tilde{u}_{\text{skm}}$ is defined by (20) and (22). The derivation of the rotation induced surface deformation, i.e., the second part of (23a), is given in Appendix B.

Also,

$$\sigma_{22}^{\text{II}} = \sigma_{12}^{\text{II}} = 0 \quad \text{for } X_2 = 0 \ |t| > l \tag{25a}$$

and the detachment condition when the cylinder rolls forward is as follows

$$-p(-l) = T_0 \tag{25b}$$

When $\sqrt{X_1^2 + X_2^2} \to \infty$,

$$\sigma_{11}^{\text{II}} = -\sigma_{11}^{\text{I}} \quad \sigma_{22}^{\text{II}} = -\sigma_{22}^{\text{I}} \quad \sigma_{12}^{\text{II}} = -\sigma_{12}^{\text{I}} \tag{26}$$

3.2 Solutions of Problem I and II. In general, according to [12] the solutions of the stress function $\Phi(z)$ for the problems I and II have the following standard form:

$$\Phi(z) = \frac{G \cdot Z(z)}{2\pi i}\int_{-l}^{l} \frac{dh(t)}{dt}\frac{dt}{Z(t)(z-t)} + Z(z)P_n(z) \tag{10'}$$

and

$$P_n(z) = C_0 + zC_1 + \cdots z^n C_1 + \cdots$$

where z is the complex plane, $z=x+iy$; $C_0, C_1, \ldots, C_n$ are constants to be determined; the boundary condition (25) requires the product $P_n(z)\cdot Z(z)$ vanishing at $z=\infty$, i.e., $P_n(z) \sim z^n$ when $Z(z) \sim z^{-(n+1)}$ at $z \to \infty$. The function $Z(z)$ is solved by enforcing $\Phi(z)$ to satisfy boundary conditions given on $n+1$ line segments. For the problems defined by Figs. 4(*a*) and 4(*b*), there is one line segment with nonzero boundary condition, i.e., (17) and (18) or (23a), (23b) on $[-l, l]$. Thus, when $n=0$, $Z(z)$ contains the singularities in the solution induced by the line segments, since, as z moves across each of them, $\Phi(z)$ has a discontinuity. Therefore, $Z(z)$ has the form as in [12]

$$Z(z) = \frac{1}{(z-l)^{(1/2)+i\beta}(z+l)^{(1/2)-i\beta}} \quad \beta = \frac{\log\kappa}{2\pi} \quad \kappa = 3 - 4v \tag{27}$$

By substituting the boundary conditions (17), (18) or (23), (24) into (10), the corresponding special solutions for problem I and II, denoted as Φ^{I} and Φ^{II}, respectively, are

$$\Phi^{\text{I}}(z,l) = \varepsilon_{\text{av}} l\left[a_1\frac{\Phi_1(z,l)}{l} + 3a_3\frac{\Phi_3(z,l)}{l^3} + \cdots\right] + i\left[\frac{\Phi_2(z,l)}{R}\right] \tag{28a}$$

$$\Phi^{\text{II}}(z,l) = \gamma_{\text{sv}}\left[2\frac{\Phi_2(z,l)}{l^2} + 4a_4\frac{\Phi_4(z,l)}{l^4} + \cdots\right] - \frac{\Delta\omega}{R}\Phi_2(z,l) + \frac{\Delta\omega^2}{2}\Phi_1(z,l) - i\Delta\omega\Phi_1(z,l) \tag{28b}$$

and

$$\Phi_{\text{stick}}(z,l) = \Phi^{\text{I}}(z,l) + \Phi^{\text{II}}(z,l) \tag{29}$$

where the constants a_i, $i=1,3,4,\ldots$, are defined in (20)–(22) and are to be determined. The solution procedure of (28*a*), (28*b*), and the detailed expression of the solved Φ_i, $i=1,2,3,4$, are given in Appendix B.

Then, by substituting Φ_{stick} into (9), one obtains

$$p(t)+iq(t)=\left\{ i\frac{k_1+\tilde{k}_1 z}{\sqrt{z^2-l^2}}+\frac{k_2+\tilde{k}_2 z}{\sqrt{z^2-l^2}}+\tilde{A}_1\sqrt{z^2-l^2}+\tilde{A}_2(z^2-l^2)^{3/2} + \tilde{A}_3 z+\cdots \right\}\left(\frac{z+l}{z-l}\right)^{i\beta}+\hat{A}_1+\hat{A}_2 z+\cdots \quad (30)$$

where $k_i, \tilde{k}_i, \tilde{A}_i, \hat{A}_i$ are constants determined by the coefficients presented in (B2)–(B9) in Appendix B.

As illustrated in Fig. 3(*b*), the first term on the right-hand side of (30) causes the same stress singularity as that at a mode I crack tip, where the coefficient k_1 corresponds to σ_0 and $\tilde{k}_1$ to the $\Delta\sigma$ that varies linearly along the crack. Similarly, the second term of (30) is analogous to the stress intensity factor caused by shear loading. They represent a pair of JKR-like singular adhesion tractions at the ends of contact zone, in the normal and transverse directions. The third term is the Hertz pressure and the remaining terms refer to the effects of nonsingular adhesion tractions and nonsymmetric loads during rolling.

3.2.1 Removal of Singularities. In order to remove the singularities that appear at $z=\pm l$ in solution (30), the following two additional constraints [13]:

$$\lim_{z\to l}[\Phi_{\text{stick}}(z,l)(z-l)^{1/2}]=0 \quad \lim_{z\to -l}[\Phi_{\text{stick}}(z,l)(z+l)^{1/2}]=0 \quad (31)$$

are applied, which lead to the two additional relations,

$$k_2+ik_1=0 \quad \tilde{k}_2+i\tilde{k}_1=0 \quad (32)$$

to determine the coefficients in (22). Subsequently, a special solution for the boundary value problem depicted by Figs. 4(*a*) and 4(*b*) is obtained. When the terms in (20)–(22) with power up to the fourth order are taken into account, this solution has the following form:

$$\Phi_{\text{stick}}(z,l)=\frac{2G}{\kappa+1}\left\{\left(\frac{z+l}{z-l}\right)^{i\beta}\sqrt{z^2-l^2}\{A_1(z^2+l^2)+A_2 z+A_3\} + A_4 z^3+A_5 z^2+A_6 z+A_7\right\} \quad (33)$$

By substituting (33) into (9), an explicit expression of the normal pressure $p(t)$ and tangential stress $q(t)$ is obtained as below:

$$p(t)+iq(t)=\frac{2G}{\kappa}\left\{[A_1(z^2+l^2)+A_2 z+A_3+B]\sqrt{z^2-l^2}\sqrt{\kappa}(1+\kappa)\cdot\left[i\cos\left[\beta\log\left(\frac{z+l}{z-l}\right)\right] - \sin\left[\beta\log\left(\frac{z+l}{z-l}\right)\right]\right]\right\} \text{ for } |t|\leqslant l \quad (34)$$

where the constants A_1, A_2, A_3, A_4, A_5, A_6, and A_7 are determined according to the three conditions in (26) and four constraints (real and imaginary parts) in (32); B is a function of A_i. These constants are solved and listed in Appendix B, expressed as the functions of the parameters l, $\Delta\omega$, γ_{sy}, ε_{av}, and a_1.

3.2.2 Determination of the Parameters. The global equilibrium conditions (15) and (16) provide three constraints for determining the coefficients in the solution (29). On the other hand, when $z\to\infty$, (33) yields the Taylor's expansion

$$\Phi_{\text{stick}}(z,l)=a_{-1}z^{-1}+a_{-2}z^{-2}+a_{-3}z^{-3}+\cdots \quad (35)$$

which satisfies (14). The coefficient a_{-1} is the residual for any closed contour integral surrounding contact zone, which equals the unbalanced forces within the contour. Hence,

$$a_{-1}=-\frac{Q+iP}{2\pi} \quad (36)$$

An additional energy conservation equation is introduced,

$$Q\cdot R\Delta\omega=\int_{-l}^{l}(u_1^{\text{II}}\cdot q(t)+u_2^{\text{II}}\cdot p(t))dt \quad (37)$$

Equations (15), (16), (36), and (37), together with the adhesion condition (25*b*), are seven equations to determine the parameters l, $\Delta\omega$, γ_{sy}, ε_{av}, a_1, and to establish the relationships between these parameters and P, Q.

Remark: For the case of steady-state rolling with stick and full sliding, the analysis procedure introduced in the previous sections is still applicable. Assuming that the roller rotates continuously with a sliding zone, within which there is no normal separation nor stick zone. Under such a steady-state the angular velocity ω should be given, denoted as a rotation angle $\Delta\tilde{\omega}$ per unit time. Similar to Fig. 4, this problem can be divided into two individual motions per unit time: (1) the roller drags the substrate moving with an angle $\Delta\omega$ due to adhesion; (2) then the deformation field of the substrate and contact zone are "frozen" while the roller rotates with the angle $\Delta\tilde{\omega}-\Delta\omega$. Hence, solutions obtained previously apply to stage (1). Stage (2) has no effect on the structures of stress and displacement distribution, although it causes extra energy dissipation. Under this condition the energy conservation (37) becomes

$$Q\cdot R\Delta\omega=\int_{-l}^{l}[(u_1+R(\Delta\tilde{\omega}-\Delta\omega))\cdot q(t)+u_2\cdot p(t)]dt \quad (37a)$$

which leads to different values of l, γ_{sy}, ε_{av} upon the input $\Delta\tilde{\omega}$.

When (31) and (32) do not apply, the singularities remain. A corresponding rolling contact solution with JKR singular adhesive traction is given by (30a), whereby the intensity of singularities, denoted as $K_{\text{I}}^{\text{coh}}$ (tension) and $K_{\text{II}}^{\text{coh}}$ (shear), respectively, are

At the front edge of the contact zone:

$$\frac{K_1^{\text{coh}}}{2G}=k_1+l\cdot\tilde{k}_1=(\alpha_{11}^{K+}+\Delta\omega\alpha_{12}^{K+})\frac{l^2}{R}+[\alpha_{13}^{K+}\gamma_{\text{sv}}\varepsilon_{\text{av}}+\alpha_{14}^{K+}\varepsilon_{\text{av}} + \alpha_{15}^{K+}\Delta\omega^2-\alpha_{16}^{K+}\Delta\omega]l \quad (38a)$$

$$\frac{K_2^{\text{coh}}}{2G}=k_2+l\cdot\tilde{k}_2=\alpha_{22}^{K+}\frac{\Delta\omega l^2}{R}+[\alpha_{23}^{K+}\gamma_{\text{sv}}\varepsilon_{\text{av}}+\alpha_{25}^{K+}\Delta\omega^2+\alpha_{26}^{K+}\Delta\omega]l \quad (38b)$$

where

$$\alpha_{11}^{K+}=-2\beta^2+\frac{1}{2} \quad \alpha_{12}^{K+}=2\beta \quad \alpha_{13}^{K+}=\frac{8\beta(2\beta^2+1)}{3}$$

$$\alpha_{14}^{K+}=-2\beta \quad \alpha_{15}^{K+}=-\beta \quad \alpha_{16}^{K+}=-1$$

$$\alpha_{22}^{K+}=-\alpha_{11}^{K+} \quad \alpha_{23}^{K+}=-\frac{1}{2}+\frac{16}{3}\beta^2-\frac{8}{3}\beta^4$$

$$\alpha_{25}^{K+}=\frac{1}{2} \quad \alpha_{26}^{K+}=-2$$

At the trailing edge of the contact zone:

$$\frac{K_1^{\text{coh}}}{2G}=k_1-l\cdot\tilde{k}_1=(\alpha_{11}^{K-}+\Delta\omega\alpha_{12}^{K-})\frac{l^2}{R}+[\alpha_{13}^{K-}\gamma_{\text{sv}}\varepsilon_{\text{av}}+\alpha_{14}^{K-}\varepsilon_{\text{av}} + \alpha_{15}^{K-}\Delta\omega^2-\alpha_{16}^{K-}\Delta\omega]l \quad (39a)$$

$$\frac{K_2^{\text{coh}}}{2G} = k_2 - l \cdot \tilde{k}_2 = \alpha_{22}^{K+}\frac{\Delta\omega l^2}{R} + [\alpha_{23}^{K+}\gamma_{sv}\varepsilon_{av} + \alpha_{25}^{K+}\Delta\omega^2 + \alpha_{26}^{K+}\Delta\omega]l \tag{39b}$$

where

$$\alpha_{11}^{K-} = \alpha_{11}^{K+} \quad \alpha_{12}^{K-} = -\alpha_{12}^{K+} \quad \alpha_{13}^{K-} = \frac{8\beta(2\beta^2-1)}{3}$$

$$\alpha_{14}^{K-} = \alpha_{14}^{K+} \quad \alpha_{15}^{K-} = \alpha_{15}^{K+} \quad \alpha_{16}^{K-} = -\alpha_{16}^{K+}$$

$$\alpha_{22}^{K-} = \alpha_{22}^{K+} \quad \alpha_{23}^{K-} = \alpha_{23}^{K+}$$

$$\alpha_{25}^{K-} = \alpha_{25}^{K+} \quad \alpha_{26}^{K-} = -\alpha_{26}^{K+}$$

Also, according to (36), one has

$$2Gk_1 = Q \quad 2Gk_2 = P \tag{40}$$

3.2.3 Friction Coefficients. According to (15) and (16), the total normal and tangential forces as well as the rolling friction coefficient

$$\mu^R = \frac{Q}{P}$$

have been obtained. Applying the coefficients listed in Appendix B, the P, Q, and μ^R can be expressed as follows:

For the solution without JKR adhesive traction:

$$\frac{P}{2G} = l\left[\alpha_{11}^P\frac{l}{R} + \alpha_{12}^P\gamma_{sv}\varepsilon_{av} + \alpha_{13}^P\varepsilon_{av} + \alpha_{14}^P(\Delta\omega)^2\right] \tag{41}$$

$$\frac{Q}{2G} = l\left[\alpha_{11}^Q\frac{l\Delta\omega}{R} + \alpha_{12}^Q\gamma_{sv}\varepsilon_{av} + \alpha_{13}^Q\Delta\omega\right] \tag{42}$$

where

$$\alpha_{11}^P = -(4\pi\beta^2 + 4\beta + \pi) \quad \alpha_{12}^P = \pi\left(\frac{16}{3}\beta^4 + \frac{8}{3}\beta^2 + 1\right)$$

$$\alpha_{13}^P = 2\alpha_{14}^P \quad \alpha_{14}^P = \kappa - 1$$

$$\alpha_{11}^Q = \alpha_{11}^P \quad \alpha_{12}^Q = 8\beta\left(4\pi\beta(\beta^2+1) + \frac{4\beta^2}{3}(1-2\pi) + \frac{2}{3}(\pi-1)\right)$$

$$\alpha_{13}^Q = -2\alpha_{14}^P$$

The corresponding rolling friction coefficient is

$$\mu_R = \frac{\dfrac{l\Delta\omega}{R} + \dfrac{\alpha_{12}^Q}{\alpha_{11}^P}\varepsilon_{av}\gamma_{sv} + \dfrac{\alpha_{13}^Q}{\alpha_{11}^P}\Delta\omega}{\dfrac{l}{R} + \dfrac{\alpha_{12}^P}{\alpha_{11}^P}\varepsilon_{av}\gamma_{sv} + \dfrac{\alpha_{13}^P}{\alpha_{11}^P}\varepsilon_{av} + \dfrac{\alpha_{14}^P}{\alpha_{11}^P}\Delta\omega^2} \tag{43}$$

For the solution with JKR adhesive traction:

$$\mu_R = \frac{\dfrac{l\Delta\omega}{R} + \alpha_{11}^\mu\varepsilon_{av}\gamma_{sv} + 2\alpha_{12}^\mu\Delta\omega}{\dfrac{l}{R} + 2\alpha_{21}^\mu\varepsilon_{av} + \alpha_{22}^\mu\Delta\omega^2} \tag{44}$$

where

$$\alpha_{11}^\mu = \frac{1}{\alpha_{22}^\mu}\left(-\frac{8}{3}\beta^4 + \frac{16}{3}\beta^2 - \frac{1}{3}\right) \quad \alpha_{12}^\mu = \alpha_{21}^\mu = -\frac{1}{\alpha_{11}^P}$$

$$\alpha_{22}^\mu = -2\beta^2 - \frac{1}{2}$$

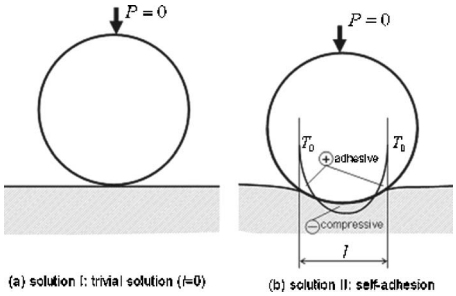

Fig. 5 Two solutions for indentation contact at $P=0$

4 Results and Discussion

4.1 The Indentation With Nonsingular Adhesion. Let $\Delta\omega = 0$, $\varepsilon_{av}=0$, the solutions (41) and (42) degenerate to a cylinder indentation contact defined by Fig. 4(*a*),

$$P = 2G\left[\alpha_{11}^P\frac{l^2}{R} + \alpha_{13}^P\varepsilon_{av}l\right] \quad Q = 0 \tag{45}$$

Applying (25*b*) to (34) (see Appendix B),

$$T_0 = \frac{2G}{\kappa}\left[(\kappa-1)\varepsilon_{av} - 2\beta\frac{l}{R}\right] \tag{46}$$

where

$$\beta = \frac{\log\kappa}{2\pi} \quad \kappa = 3 - 4v$$

Combining (45) with (46), the unknown ε_{av} is cancelled and the resulting relation below establishes the relationship among contact zone size, applied normal load, and maximum adhesion,

$$l = \frac{T_0R\kappa}{2G\pi(1+4\beta^2)}\left[1 + \sqrt{1 - \frac{4\pi(\beta^2+1)}{\kappa}\left(\frac{PG}{RT_0^2}\right)}\right] \tag{47}$$

When no external force is applied, i.e., $P=0$, two bifurcated solutions of l, as illustrated in Fig. 5, are obtained,

$$\text{Solution I(trivial):} \quad l = \varepsilon_{av} = 0$$

$$\text{Solution II:} \quad l = \frac{2(\kappa-1)}{4\pi\beta^2 + 4\beta + \pi}R\varepsilon_{av}$$

By substituting the second solution into (46), we reach the following estimate of the relation between contact zone size and maximum adhesion which is exact when no external force and the system is under infinitesimal deformation,

$$T_0 = \frac{\pi G}{\kappa}(4\beta^2+1)\frac{l}{R} \tag{47a}$$

or

$$l = \frac{T_0R}{\pi G(4\beta^2+1)} \tag{47b}$$

4.2 The Rolling-Contact Solution With Adhesion. We focus on the nonsingular solutions given in the previous section. The major results are plotted in Figs. 6–9. Figures 6(*a*) and 6(*b*) display the relationships between ε_{av} and $\Delta\omega$ under small applied normal load for substrates with varying Poisson's ratio, where ε_{av} characterizes the average surface transverse strain and $\Delta\omega$ stands for the rotation deformation during rolling and the enhanced process of attachment–adhesion–detachment. In these two diagrams the normal load is represented by a dimensionless parameter $\bar{P}$, $\bar{P}=P/(bRG)$; b is thickness, where $b=1$ is assumed for the plane strain condition, R is the radius of the roller, and G is the Young's

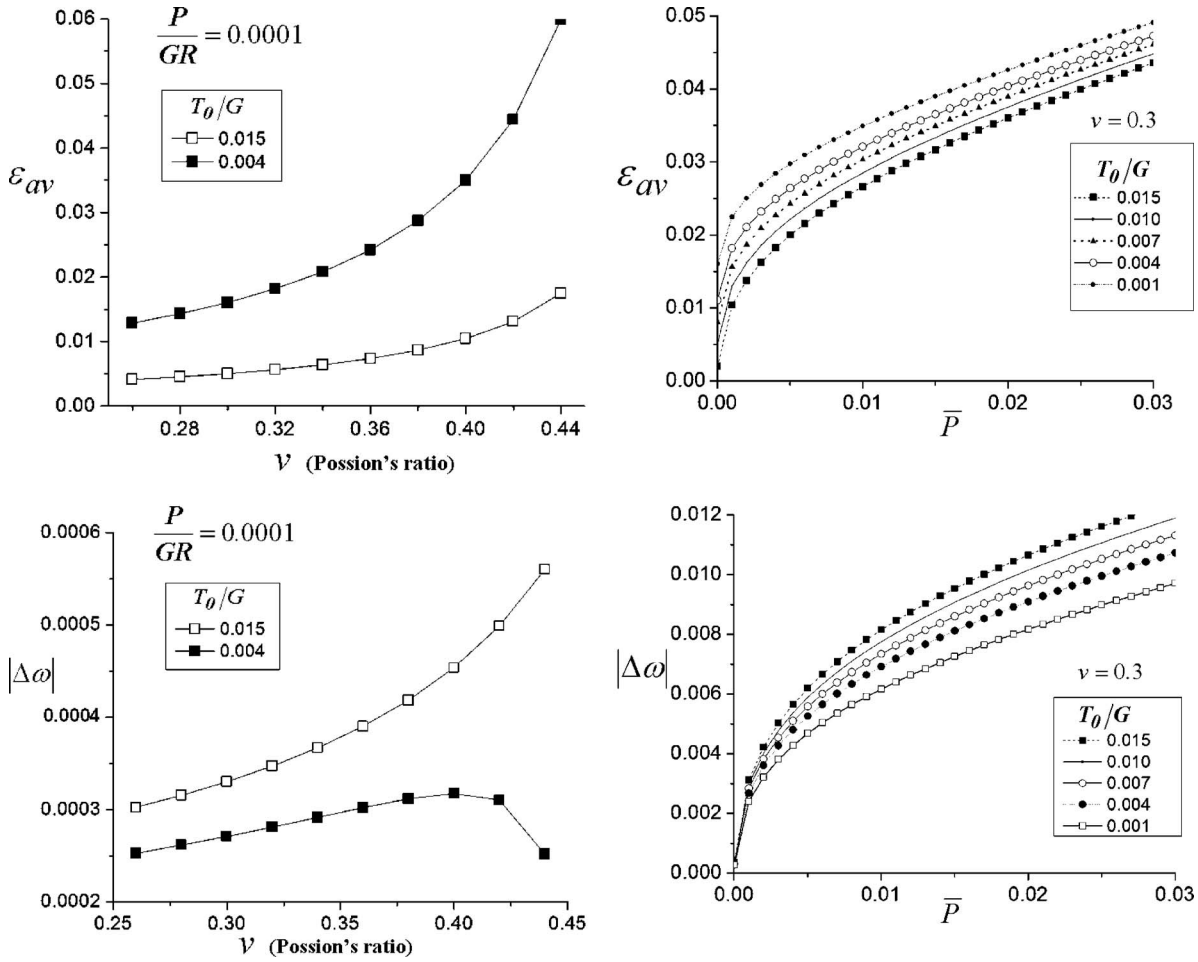

Fig. 6 The solutions of (*a*) the average transverse surface contact strain ε_{av} vs Poisson's ratio at small normal load; (*b*) the rotation angle $\Delta\omega$ vs Poisson's ratio at small normal load; (*c*) the evolution of ε_{av} when normalized load $\bar{P}$ increases; (*d*) the evolution of $\Delta\omega$ as $\bar{P}$ increases

modulus. Figure 6(*a*) shows that under the same normal load the average transverse strain on the contact surface (ε_{av}) increases monotonically when the value of the substrate Poisson's ratio rises. On other hand, ε_{av} is smaller when T_0, and the maximum adhesion defined in (1), is higher. This phenomenon is consistent with the results shown in Fig. 6(*b*) in which the relations between Poisson's ratio and the maximum nondetachment rotation angle $\Delta\omega$ are given. It shows that a smaller adhesion leads to a smaller $\Delta\omega$ since a detachment will occur earlier. These conclusions are confirmed by the results in Figs. 6(*c*) and 6(*d*) in which the evolution of ε_{av} and $\Delta\omega$ for varying T_0 are plotted when the normal applied load rises. From Figs. 6(*a*) and 6(*b*) one can also conclude that the Possion's ratio essentially reflects the deformability of the contact surface. A higher Possion's ratio leads to a higher surface transverse strain and nondetachment rotation angle. However, Fig. 6(*b*) reveals a bifurcated phenomenon that, when adhesion is weak and the Possion's ratio approaches 0.5 (>0.4), detachment tends to occur earlier. These seem to imply that plastic deformation may cause higher drag force to detach.

Figures 7(*a*) and 7(*b*) display the comparisons of normal and shear stress on the contact surface, respectively, between the derived rolling-sliding-stick solution and the Hertz solution (without rolling), where the stresses are normalized by a denominator, $2G/\kappa$. A significant difference in the tangential stress distribution (Fig. 7(*b*)) can be seen where the shear stress under rolling-contact exhibits an oscillating behavior in the first half of the contact zone towards the direction of rolling. The distribution of normal stresses for rolling contact shows a similar trend as in the case of the Hertz contact. However, in the adhesion case the distribution is no longer symmetric and a tension stress zone emerges near the tail to X^{a-} within which the adhesion is effective to sustain the contact surfaces sticking together during rolling-rotation deformation. Although the deviation from the Hertz's solution is moderate, a decisive difference in the contact process is caused.

Plotted in Fig. 8 are snapshots of the normal and shear stresses under varying loads. Figure 8(*a*), displayed for the case of $T_0/G = 0.01$, demonstrates that the normal stress distribution gradually deviates from the Hertz solution and is more concentrated in the side close to the trailing edge of the contact zone when the applied load decreases. This phenomenon is caused by the effect of tensile stress on the trailing edge of the contact zone due to adhesion. When the load is lower, additional pressure is required to keep the system in equilibrium. Obviously, the reduction of normal stress decreases the corresponding shear stress. Hence, an additional "half-wave" of the tangential stress distribution with small amplitude on the side opposite to the trailing edge appears, as demonstrated in Figs. 7 and 8. Also, the plots in Fig. 8 show that the stress distributions are somewhat deviated from "self-similar" when applied load varies. This is caused by the second order term, e.g., $\Delta\omega^2$, in (35)–(37) and in (41)–(44); which leads to a nonlinear relationship to the applied load, as plotted in Figs. 6(*c*) and 6(*d*).

In general, the obtained solution can be interpreted as a JKR-

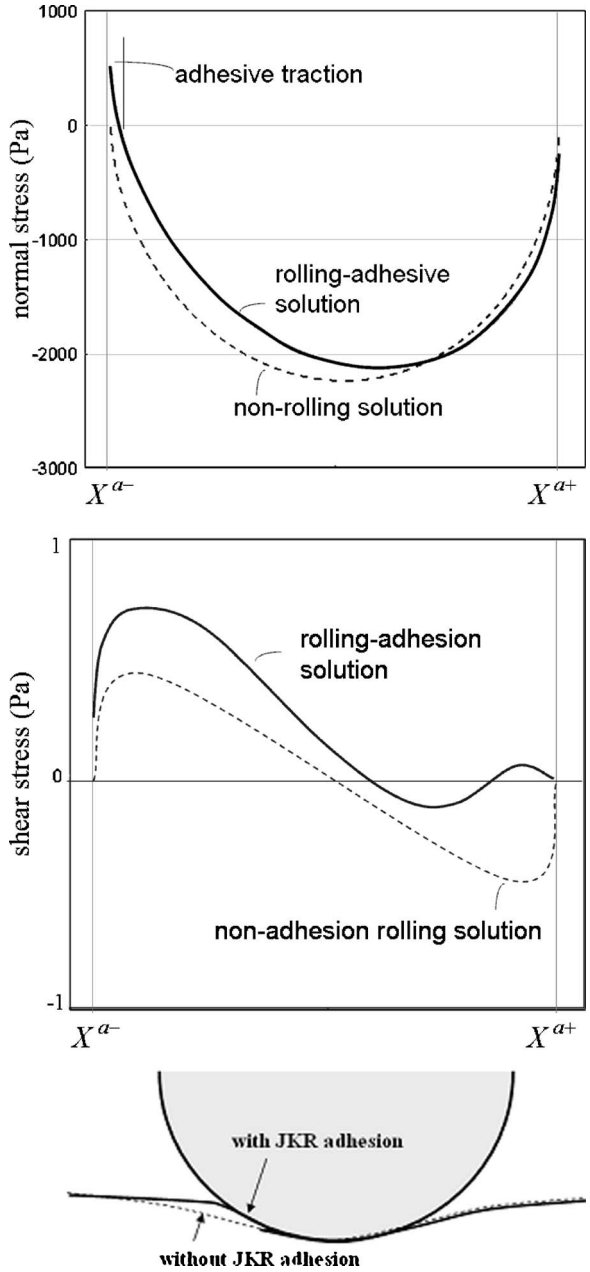

Fig. 7 Comparison between rolling and nonrolling solutions for the normal stress and shear stress: (*a*) normal stress; (*b*) shear stress; (*c*) illustration of the deformation

type rolling adhesion contact solution without singularity, or a Hertz-type rolling contact solution with adhesion.

4.3 Resultant Moment and Definition of Friction Coefficient. The rolling friction coefficient μ_R, defined as the ratio between transverse resistance and normal pressure and explicitly expressed by (43), has also been computed. The results are plotted in Fig. 9 which shows that μ_R is no longer a constant but can vary with load. According to this diagram one concludes that adhesion is a major cause of friction resistance during rolling contact, since it keeps the substrate attached to the cylinder roller. When the normal load is very small, the adhesion force dominates the contact, which leads to higher friction resistance. Whereas, when the applied normal load increases, the portion due to adhesion reduces; so the effects of adhesion fade and the friction resistance decreases. Plotted in Fig. 10 are the relationship among maximum adhesion, total normal compression force, and the corresponding resultant moment. The left half of the diagram is the relationship between resultant moment and adhesion when normal compression is not present. The right half of the diagram is that between moment and normal force under given maximum adhesion, which shows a trend toward linearity when $\bar{P}$ is not small.

Therefore, an "adhesion friction coefficient" defined below is proposed to characterize the capability of a surface to resist a rolling motion under these situations,

$$\mu^A = \frac{Q}{T_0 R \kappa^A + P} \tag{48}$$

where R is the radius of the roller, Q is the friction resistance force that is parallel to the rolling/sliding direction, P is the applied force perpendicular to the rolling direction; T_0 is the maximum adhesion per unit area; κ^A is a coefficient that related to the area on which adhesion is present. Hence, κ^A is a function of the Young's modulus of substrate and the decohesion law during adhesive contact. After performing numerical regression based on the theoretical solutions obtained in this paper, the following expression of κ^A has been obtained when nonsingular adhesion is present:

$$\kappa^A = \frac{T_0}{6bG} \tag{49}$$

where G is shear Young's modulus and b is the thickness, $b=1$ for plane strain.

5 Conclusions

In this analysis a procedure to obtain an analytical solution of rolling contact with adhesion has been proposed and two solutions have been obtained. In the first solution an adhesion law characterized by a finite maximum adhesive traction is applied, which essentially governs the process of attachment-adhesion-detachment during rolling. The solution with JKR singular adhesive traction has also been derived. By assuming the rotation angle to be zero, the first solution degenerates to a solution of the indentation contact with finite adhesion. From these theoretical analyses the following conclusions have been obtained:

(1) The stress field obtained reveals that normal stress distribution in the contact zone is different from the Hertz solution due to the presence of a tensile stress that causes the contact surfaces to stick together and induces additional normal pressure to maintain the system equilibrium. As the amplitude of the externally applied normal pressure increases, the effects of adhesion recedes and the stress distribution exhibits a trend towards the Hertz solution. Hence, the derived solution can be considered as a JKR-type rolling adhesion contact solution without singularity, or a Hertz-type rolling contact solution with adhesion.

(2) By assuming the rotation angle to be zero, the obtained rolling contact solution degenerates to a solution of the indentation contact with finite adhesion. This solution reveals "dual states" when no external applied load: the indent will either stay as "point" contact or form a self-adhesive system. When the second case takes place, the following solution (Eq. (47*b*)) of the contact zone size has been obtained:

$$l = \frac{T_0 R}{\pi G(4\beta^2 + 1)}$$

if the system is under infinitesimal deformation; in (47*b*) R is the radius of the roller, T_0 is the maximum adhesion per unit area, G is the shear modulus, and β is a material constant correlated to Possion's ratio.

(3) From the solutions the expression of rolling coefficients, defined as the ratio of the transverse friction resistance and normal pressure, have been obtained and are listed in (43) and (44). These relations, in conjunction with (47*b*) and the

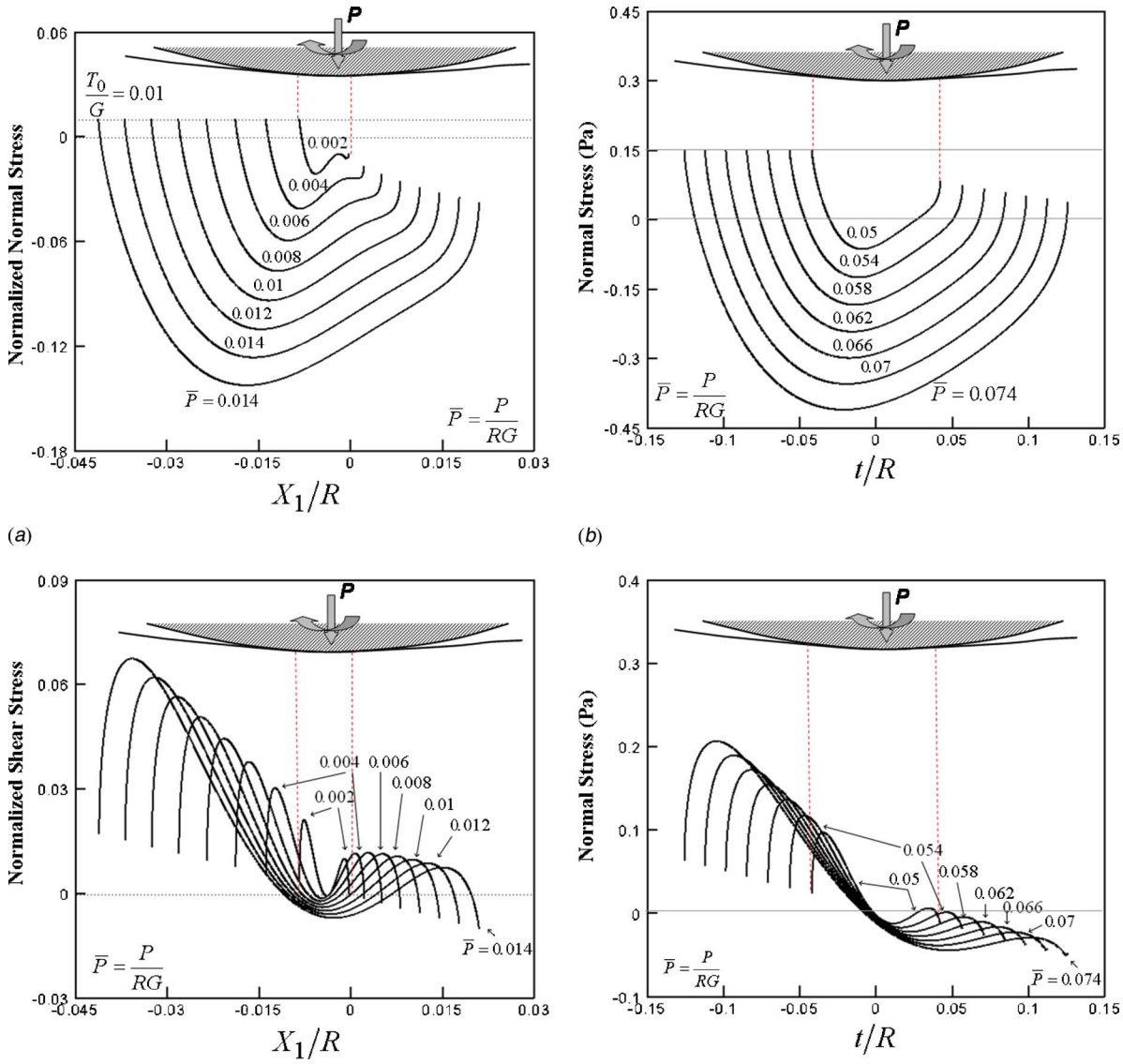

Fig. 8 The solved normal pressure and shear stress distributions in contact-stick zone, varying with applied normal load: (*a*) the stresses plotted in the $\{X_i\}$ coordinate system for the case of $T_0/G=0.01$, small applied normal load; (*b*) the stresses plotted in the $\{t\}$ coordinate system for the case of $T_0/G=0.15$ under moderate normal load

results plotted in Fig. 9 reveal that the rolling-stick contact is a complex process with energy dissipation, the conventional friction coefficient, defined as the ratio between tangential resistance and normal compressive force, is not sufficient to describe the physics involved in this process. In order to characterize the adhesion-friction behavior under this situation, this paper suggests an "adhesion friction coefficient" for plane strain rolling contact with nonsingular adhesion that is defined by

$$\mu^A = \frac{Q}{T_0^2 R/(6G) + P} \tag{48'}$$

where Q is the friction resistance force, parallel to the rolling/sliding direction; P is the applied force normal to the rolling direction [34,35].

Appendix A: The Boundary Condition (23)

According to the geometric relation illustrated in Fig. 11, the horizontal and vertical displacements, denoted as u^{II} and v^{II}, respectively, can be expressed as

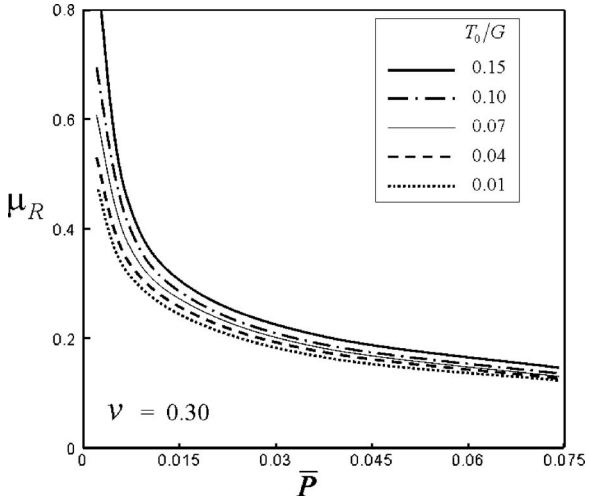

Fig. 9 The solved rolling-stick friction coefficient (37*a*) against normalized load under different JKR adhesion

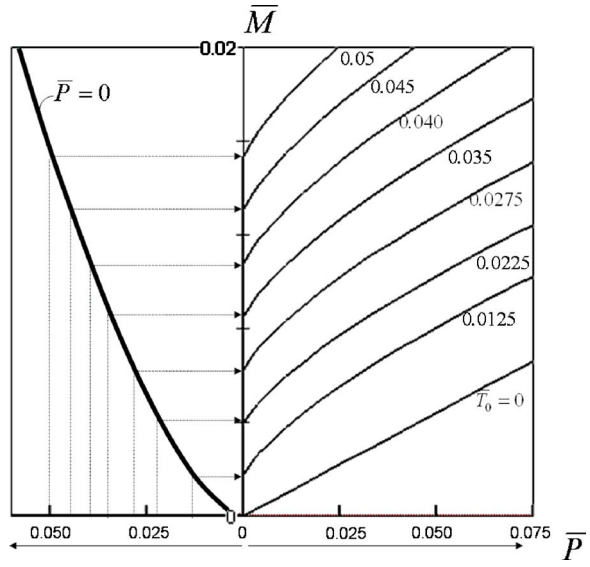

Fig. 10 The relationship among maximum adhesion T_0, total normal compression force P, and the corresponding resultant moment M, where $\bar{T}_0=T_0/(6G)$, $\bar{P}=P/(RG)$, $\bar{M}=M/(RbG)$, and $b=1$ for the plane strain

$$u^{\mathrm{II}}=2R\sin\left(\frac{\Delta\omega}{2}\right)\cos\left(\frac{\Delta\omega}{2}+\theta\right)\quad v^{\mathrm{II}}=2R\sin\left(\frac{\Delta\omega}{2}\right)\sin\left(\frac{\Delta\omega}{2}+\theta\right) \tag{A1}$$

Applying the Talyor's expansions

$$\sin\Delta\omega=\Delta\omega-\frac{\Delta\omega^3}{3!}+\cdots\quad\cos\Delta\omega=1-\frac{\Delta\omega^2}{2!}+\cdots \tag{A2}$$

and

$$\theta=\frac{t}{R} \tag{A3}$$

substituting (A2) and (A3) into (A1), and leaving out the high order small terms in the above relations one obtains:

According to the geometric relation illustrated in Fig. 11, the horizontal and vertical displacements, denoted as u and v, respectively, can be expressed as

$$u=2R\sin\left(\frac{\Delta\omega}{2}\right)\cos\left(\frac{\Delta\omega}{2}+\theta\right)\quad v=2R\sin\left(\frac{\Delta\omega}{2}\right)\sin\left(\frac{\Delta\omega}{2}+\theta\right) \tag{A1$'$}$$

Applying the Talyor's expansions

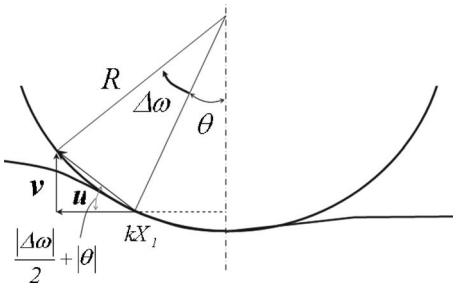

Fig. 11 Geometric relationship between stick-rotation angle $\Delta\omega$ and displacement increments

$$\sin\Delta\omega=\Delta\omega-\frac{\Delta\omega^3}{3!}+\cdots\quad\cos\Delta\omega=1-\frac{\Delta\omega^2}{2!}+\cdots \tag{A2$'$}$$

and

$$\theta=\frac{t}{R} \tag{A3$'$}$$

substituting (A2) and (A3) into (A1) and leaving out the high order small terms in the above relations one obtains

$$u=R\Delta\omega\left[\left(1-\frac{1}{2}\left(\frac{t}{R}\right)^2-\frac{\Delta\omega^2}{6}\right)+\frac{t}{R}\frac{\Delta\omega}{2}\right]\quad\text{for } X_2=0,\quad |t|\leqslant l \tag{A4}$$

$$v=R\Delta\omega\left[\frac{\Delta\omega}{2}-\frac{t}{R}\right]\quad\text{for } X_2=0,\quad |t|\leqslant l \tag{A5}$$

Appendix B: A Brief Introduction of the Solution Procedure to Obtain (27)–(30)

Considering the integration equation, e.g., the first term on the right-hand side of (10)

$$\Phi(z)=\frac{G\cdot Z(z)}{2\pi i}\int_{-l}^{l}\frac{dh(t)}{dt}\frac{dt}{Z(t)(z-t)} \tag{B1}$$

where the function $Z(z)$ is defined by (27). When the coordinate z moves along a path surrounding the singular point $\{l,0\}$ or $\{-l,0\}$ from one side of the line segment $\{|x|=|t|\leqslant l, y=0\}$ to another side, $Z(z)$ obtains the increment with the amplitude $|\kappa|$.

The displacement within the contact zone, denoted as $h(t)$ in (B1),

$$h(t)=u_1(t)+iu_2(t)\quad\text{at } X_2=0\ |t|\leqslant l \tag{B2}$$

essentially determines the final form of the stress function $\Phi(z)$. When it has the following simple forms, respectively,

$$h_1(t)=t\quad h_2(t)=t^2\quad h_3(t)=t^3\quad h_4(t)=t^4 \tag{B3}$$

the corresponding special solutions of (B1) are, respectively,

$$\Phi_1(z,l)=\frac{2G}{\kappa+1}\left\{1-\frac{(z-2i\beta l)}{\sqrt{z^2-l^2}}\left(\frac{z+l}{z-l}\right)^{i\beta}\right\} \tag{B4}$$

$$\Phi_2(z,l)=\frac{2G}{(\kappa+1)}\left\{z-\left[\frac{2z^2-4i\beta lz-(1+4\beta^2)l^2}{2\sqrt{z^2-l^2}}\right]\left(\frac{z+l}{z-l}\right)^{i\beta}\right\} \tag{B5}$$

$$\Phi_3(z,l)=\frac{2G}{(\kappa+1)}\left\{z^2-\left[\frac{z^3-2i\beta lz^2-\left(\frac{1}{2}+2\beta^2\right)zl^2+i\left(\frac{1}{3}+\frac{4}{3}\beta^2\right)\beta l^3}{\sqrt{z^2-l^2}}\right]\left(\frac{z+l}{z-l}\right)^{i\beta}\right\} \tag{B6}$$

$$\Phi_4(z,l)=\frac{2G}{(\kappa+1)}\left\{z^3-\left(\frac{z+l}{z-l}\right)^{i\beta}\cdot\left[\frac{z^4-2i\beta lz^3-\left(\frac{1}{2}+2\beta^2\right)z^2l^2+i\left(\frac{1}{3}+\frac{4}{3}\beta^2\right)\beta zl^3-\left(\frac{1}{8}+\frac{1}{3}\beta^2-\frac{2}{3}\beta^4\right)l^4}{\sqrt{z^2-l^2}}\right]\right\} \tag{B7}$$

where $\beta=\log\kappa/2\pi$ is the material constant determined by Poisson's ratio. Equations (B2)–(B7) can be proven using the method introduced in (Note 1 of Sec. 110 in [12]).

For the solution (33)

$$\Phi_{\text{stick}}(z,l)=\frac{2G}{\kappa+1}\left\{\left(\frac{z+l}{z-l}\right)^{i\beta}\sqrt{z^2-l^2}\{A_1(z^2+l^2)+A_2z+A_3\}+A_4z^3+A_5z^2+A_6z+A_7\right\}$$

applying (26) and (32) the coefficients are as below:

$$A_1=\frac{4\varepsilon_{\text{av}}\gamma_{\text{sv}}}{l^3}\quad A_2=-\frac{8\varepsilon_{\text{av}}\gamma_{\text{sv}}i\beta}{l^2}+\frac{(-3+3a_1)\varepsilon_{\text{av}}}{l^2}$$

$$A_3=\left(\frac{6(1-a_1)\beta\varepsilon_{\text{av}}}{l}-\frac{1}{R}\right)i+\frac{\left(-2\gamma_{\text{sv}}-4\gamma_{\text{sv}}\left(\frac{1}{2}+2\beta^2\right)\right)\varepsilon_{\text{av}}}{l}+\frac{\Delta\omega}{R}$$

$$A_4=-\frac{4\varepsilon_{\text{av}}\gamma_{\text{sv}}}{l^3}$$

$$A_5=\frac{3(1-a_1)\varepsilon_{\text{av}}}{l^2}\quad A_6=\frac{i}{R}+\frac{2\varepsilon_{\text{av}}\gamma_{\text{sv}}}{l}-\frac{\Delta\omega}{R}$$

$$A_7=\frac{-2\beta l}{R}-\left(\left(4\gamma_{\text{sv}}\beta-4\gamma_{\text{sv}}\left(\frac{1}{3}\beta+\frac{4}{3}\beta^3\right)\right)\varepsilon_{\text{av}}+\left(-1+\frac{2\beta l}{R}\right)\Delta\omega\right)i-\left(3-2a_1-3(1-a_1)\left(\frac{1}{2}+2\beta^2\right)\right)\varepsilon_{\text{av}}-\frac{\Delta\omega^2}{2} \tag{B8}$$

The corresponding pressure and tangent shear are (Eq. (34))

$$p(t)+iq(t)=\frac{2G}{\kappa}\left\{[A_1(z^2+l^2)+A_2z+A_3+B]\sqrt{z^2-l^2}\sqrt{\kappa}(1+\kappa)\cdot\left[i\cos\left[\beta\log\left(\frac{z+l}{z-l}\right)\right]-\sin\left[\beta\log\left(\frac{z+l}{z-l}\right)\right]\right]\right\}\quad\text{for } |t|\leqslant l$$

where A_1, A_2, A_3 are given by (B8) and

$$B=\frac{8\varepsilon_{\text{av}}\gamma_{\text{sv}}\beta z}{l^2}-\frac{6(1-a_1)\beta\varepsilon_{\text{av}}}{l}+\frac{1}{R}+i\left(\frac{4\varepsilon_{\text{av}}\gamma_{\text{sv}}(z^2+l^2)}{l^3}+\frac{(-3+3a_1)\varepsilon_{\text{av}}z}{l^2}+\frac{\left(-2\gamma_{\text{sv}}-4\gamma_{\text{sv}}\left(\frac{1}{2}+2\beta^2\right)\right)\varepsilon_{\text{av}}}{l}+\frac{\Delta\omega}{R}\right)$$

When the cylinder rolls forward, the detachment condition (25*b*) has to be satisfied,

$$-p(-l)=T_0$$

By substituting (34) into this relation,

$$T_0=2G\left(\left(2(\kappa-1)\gamma_{\text{sv}}+3(\kappa-1)(1-a_1)+3(1-a_1)\left(\frac{1}{2}+2\beta^2\right)+2\gamma_{\text{sv}}+(\kappa-1)a_1\right)\varepsilon_{\text{av}}+\frac{(\kappa-1)\Delta\omega^2}{2}+\frac{(-2\beta+\Delta\omega+(\kappa-1)\Delta\omega)l}{R}\right)\Big/\kappa \tag{B9}$$

Also, the numerical solution shows that $a_1=1-\Delta$ where $|\Delta|\leqslant 2e-2$. So in the analysis, the following relation has been taken:

$$a_1\approx 1 \tag{B10}$$

References

[1] Hertz, H., 1882, "On the Contact of Elastic Solids," J. Reine Angew. Math., **92**, pp. 156–170.

[2] Greenwood, J. A., and Williams, J. B., 1966, "Contact of Nominally Flat Surfaces," Proc. R. Soc. London, Ser. A, **295**(1442), pp. 300–394.

[3] Johnson, K. L., 1985, *Contact Mechanics*, Cambridge University Press, Cambridge, UK, Chap. 8.

[4] Maugis, D., 1999, *Contact, Adhesion and Rupture of Elastic Solids*, Springer-Verlag, Berlin, Germany, Chaps. 3–4.

[5] Chen, Y. H., Polonsky, I. A., Chung, Y. W., and Keer, L. M., 2002, "Tribological Properties and Rolling-Contact-Fatigue Lives of TiN/SiNx Multilayer Coatings," Surf. Coat. Technol., **154**(2–3), pp. 152–161.

[6] Veprek, S., Mukherjee, S., Karvankova, P., Männling, H. D., He, J. L., Moto, K., Prochazka, J., and Argon, A. S., 2003, "Hertzian Analysis of the Self-Consistency and Reliability of the Indentation Hardness Measurements on Superhard Nanocomposite Coatings," Thin Solid Films, **436**(2), pp. 220–231.

[7] Tayebi, N., and Polycarpou, A. A., 2005, "Reducing the Effects of Adhesion and Friction in Microelectromechanical Systems (MEMSs) Through Surface Roughening: Comparison Between Theory and Experiments," J. Appl. Phys., **98**(7), p. 073528.

[8] Sari, O. T., Adams, G. G., and Muftu, S., 2005, "Nano-Scale Effects in the Sliding and Rolling of a Cylinder on a Substrate," ASME J. Appl. Mech., **72**(5), pp. 633–640.

[9] Shi, X., and Polycarpou, A. A., 2005, "An Elastic-Plastic Hybrid Adhesion Model for Contacting Rough Surfaces in the Presence of Molecularly Thin Lubricant," J. Colloid Interface Sci., **290**(2), pp. 514–525.

[10] Burfler, H., 1959, "Theorie der rollenden Reibung," Ing.-Arch., **27**, pp. 207–247.

[11] Carter, F. W., 1926, "On the Action of a Locomotive Driving Wheel," Proc. R. Soc. London, Ser. A, **112**, pp. 151–157; more detail description can be found in Chap. 12 of [33].

[12] Muskhelishvili, N. I., 1953, *Some Basic Problems of the Mathematical Theory of Elasticity*, 3rd ed., P. Noordhoff, Groningen, Chaps. 17–19.

[13] Achenbach, J. D., Keer, L. M., Khetan, R. P., and Chen, S. H., 1979, "Loss of Adhesion at the Tip of an Interface Crack," J. Elast., **9**(4), pp. 397–424.

[14] Dugdale, D. S., 1960, "Yielding of Steel Sheets Containing Slits," J. Mech. Phys. Solids, **8**(2), pp. 100–104.

[15] Johnson, K. L., Kendall, K., and Roberts, A. D., 1971, "Surface Energy and Contact of Elastic Solids," Proc. R. Soc. London, Ser. A, **324**(1558), pp. 301–342.

[16] Derjaguin, B. V., Muller, V. M., and Toporov, M., 1975, "Effect of Contact Deformations on Adhesion of Particles," J. Colloid Interface Sci., **53**(2), pp. 314–326.

[17] Hughes, B. D., and White, L. R., 1979, "Soft Contact Problems in Linear Elasticity," Q. J. Mech. Appl. Math., **32**, pp. 445–471.

[18] Barquins, M., 1988, "Adherence and Rolling Kinetics of a Rigid Cylinder in Contact With a Natural Rubber Surface," J. Adhes., **26**(1), pp. 1–12.

[19] Baney, J. M., and Hui, C.-Y., 1997, "A Cohesive Zone Model for the Adhesion of Cylinder," J. Adhes. Sci. Technol., **11**, pp. 393–406.

[20] Chen, S. H., and Gao, H. J., 2006, "Non-Slipping Adhesive Contact of an Elastic Cylinder on Stretched Substrates," Proc. R. Soc. London, Ser. A, **462**(2065), pp. 211–228.

[21] Spence, D. A., 1968, "Self Similar Solutions to Adhesive Contact Problems With Incremental Loading," Proc. R. Soc. London, Ser. A, **305**(1480), pp. 55–74.

[22] Hasebe, N., and Qian, J., 1999, "Fundamental Solution of a Circular Rigid Punch Problem for a Half Plane," Eng. Anal. Boundary Elem., **23**, pp. 841–846.

[23] Hasebe, N., Okumura, M., and Nakamura, T., 1989, "Frictional Punch and Crack in Plane Elasticity," J. Eng. Mech., **115**, pp. 1137–1149.
[24] Borodich, F. M., and Keer, L. M., 2004, "Contact Problems and Depth-Sensing Nanoindentation for Frictionless and Frictional Boundary Conditions," Int. J. Solids Struct., **41**(9–10), pp. 2479–2499.
[25] Borodich, F. M., and Keer, L. M., 2004, "Evaluation of Elastic Modulus of Materials by Adhesive (No-Slip) Nano-Indentation," Proc. R. Soc. London, Ser. A, **460**(2042), pp. 507–514.
[26] Mossakovskii, V. I., 1954, "The Fundamental Mixed Problem of the Theory of Elasticity for a Half-Space With a Circular Line Separating the Boundary Conditions," J. Appl. Math. Mech., **18**, pp. 187–196.
[27] Kim, K. S., McMeeking, R. M., and Johnson, K. L., 1998, "Adhesion, Slip, Cohesive Zones and Energy Fluxes for Elastic Spheres in Contact," J. Mech. Phys. Solids, **46**(2), pp. 243–266.
[28] Greenwood, J. A., and Johnson, K. L., 1998, "An Alternative to the Maugis Model of Adhesion Between Elastic Spheres," J. Phys. D, **31**(22), pp. 3279–3290.
[29] Johnson, K. L., and Greenwood, J. A., 1998, "An Adhesion Map for the Contact of Elastic Spheres," J. Colloid Interface Sci., **192**(2), pp. 326–333.
[30] Yao, H., and Gao, H. J., 2006, "Mechanics of Robust and Releasable Adhesion in Biology: Bottom-up Designed Hierarchical Structures of Gecko," J. Mech. Phys. Solids, **54**(6), pp. 1120–1146.
[31] Needleman, A., 1987, "A Continuum Model for Void Nucleation by Inclusion Debonding," ASME J. Appl. Mech., **54**(3), pp. 525–531.
[32] Hao, S., Liu, W. L., Moran, B., and Olson, G. B., 2003, "A Hierarchical Multi-Physics Constitutive Model for Steels Design," Comput. Methods Appl. Mech. Eng., **193**(17–20), pp. 1865–1908.
[33] Barber, J. R., 2003, *Elasticity*, 2nd ed., Kluwer Academic, Dordrecht, Netherlands, Chap. 12.
[34] Hamaker, H. C., 1937, "The London—Van Der Waals Attraction Between Spherical Particles," Physica (Amsterdam), **4**(10), pp. 1058–1072.
[35] Kogut, L., and Etsion, I., 2004, "A Static Friction Model for Elastic-Plastic Contacting Rough Surface," ASME J. Tribol., **126**, pp. 34–40.